

MINERALOGICAL MAGAZINE

VOLUME 58

NUMBER 391

JUNE 1994

An EXAFS study of cation site distortions through the $P2/c$ – $P\bar{1}$ phase transition in the synthetic cuproscheelite–sanmartinite solid solution

P. F. SCHOFIELD*, J. M. CHARNOCK, G. CRESSEY¹ AND C. M. B. HENDERSON

Department of Geology, University of Manchester, Oxford Road, Manchester M13 9PL, UK

¹Department of Mineralogy, Natural History Museum, Cromwell Road, London SW7 5BD, UK

Abstract

EXAFS spectroscopy has been used to monitor changes in divalent cation site geometries across the $P2/c$ – $P\bar{1}$ phase transition in the sanmartinite (ZnWO_4)–cuproscheelite (CuWO_4) solid solution at ambient and liquid nitrogen temperatures. In the ZnWO_4 end member, Zn occupies axially-compressed ZnO_6 octahedra with two axial Zn–O bonds at approximately 1.95 Å and four square planar Zn–O bonds at approximately 2.11 Å. The substitution of Zn by Cu generates a second Zn environment with four short square planar Zn–O bonds and two longer axial Zn–O bonds. The proportion of the latter site increases progressively as the Cu content increases. Cu EXAFS reveals that the CuO_6 octahedra maintain their Jahn-Teller axially-elongate geometry throughout the majority of the solid solution and only occur as axially-compressed octahedra well within the stability field of the Zn-rich phase with monoclinic long-range order.

KEYWORDS: EXAFS spectroscopy, sanmartinite, cuproscheelite, phase transition.

Introduction

RECENT powder X-ray diffraction studies on the complete solid solution between sanmartinite, ZnWO_4 , and cuproscheelite, CuWO_4 , have revealed the existence of a displacive ferroelastic phase transition (Schofield and Redfern, 1992, 1993). The spontaneous strain, calculated from the lattice parameters, was used as a measure of the order parameter for the transition which, at room

temperature, appeared continuous as a function of composition and with a critical composition of $\text{Cu}_{0.22}\text{Zn}_{0.78}\text{WO}_4$. With increasing Cu-content and temperature, the transition was found to become more first-order in character with a tricritical transition occurring at about $\text{Zn}_{0.32}\text{Cu}_{0.68}\text{WO}_4$ and 650°C. The observed critical transition temperature varied non-linearly as a function of composition indicating a coupling between X , the molar fraction CuWO_4 , and the order parameter, Q , of the form $\zeta_1 X Q^2 + \zeta_2 X Q^4$. The resulting Landau potential successfully modelled the transition as a function of both composition and temperature.

*Present Address: Department of Mineralogy, Natural History Museum, Cromwell Road, London SW7 5BD, UK

The long-range information obtained from these diffraction experiments gives no indication of the nature of the cation site distortions across the solid solution; in this paper we will describe the long-range length scale probed by X-ray diffraction as 'macroscopic'. By contrast, element specific X-ray absorption spectroscopy probes the short-range order (i.e. a few Å); we will describe this length scale as 'microscopic'. The Cu $2p$ X-ray absorption spectroscopy (Schofield *et al.*, 1993) indicates that the inclusion of Zn into the CuWO_4 structure generates a second Cu electronic site. The relative proportions of the two Cu sites, present as microscopically triclinic-type and monoclinic-type sites, varies continuously across the solid solution and the mole fractions of the two sites enable the site occupancies to be successfully modelled. The precise nature of these two Cu sites cannot be elucidated fully until further information is obtained about their geometrical variation, and the coupled interaction with the Zn site across the solid solution. Extended X-ray Absorption Fine Structure (EXAFS) spectroscopy has been shown to be an excellent tool for probing site

environments by providing essentially one-dimensional, radial information on bond distances, coordination numbers and disorder properties of shells of atoms surrounding the central target atom (Brown *et al.*, 1988). In the present paper we have used this technique to monitor Cu and Zn site geometries as Zn is substituted by Cu in the series $\text{ZnWO}_4\text{-CuWO}_4$.

Crystal structures

Filipenko *et al.* (1968) refined the structure of ZnWO_4 showing it to have the monoclinic wolframite structure with space group $P2_1/c$ and two formula units per unit cell. This structure (Fig. 1) consists of infinite zig-zag chains, running parallel to $[001]$, composed entirely of either edge-sharing ZnO_6 octahedra or WO_6 octahedra. Each chain of ZnO_6 octahedra is corner-linked to four chains of WO_6 octahedra, and vice-versa, leaving open channels parallel to the z -axis.

Although CuWO_4 is triclinic with a space group $P\bar{1}$, Kihlborg and Gebert (1970) and later Klein and Weitzel (1975) have shown this

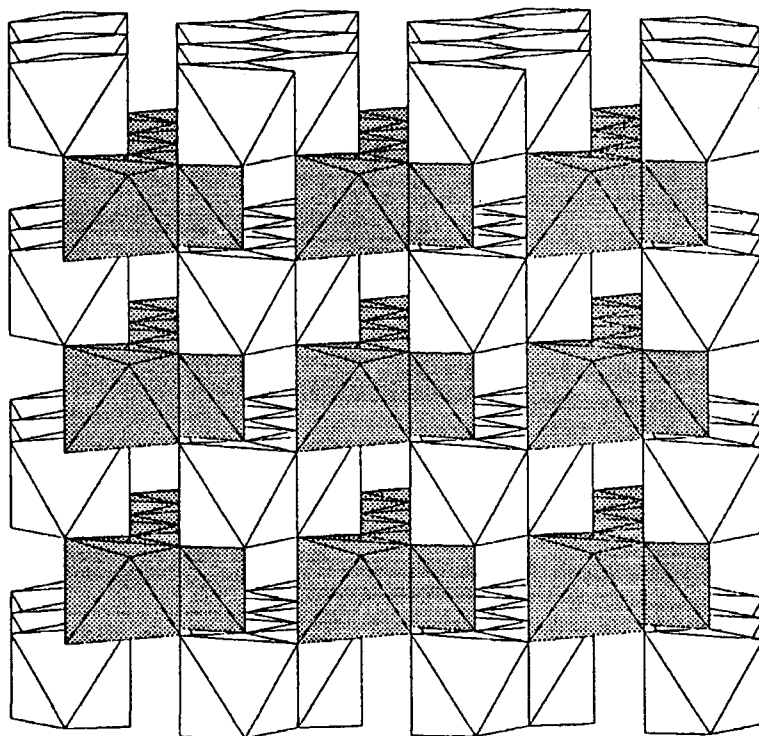


FIG. 1. A polyhedral representation of the ZnWO_4 structure viewed along the z -axis. Shaded octahedra represent WO_6 octahedra. x -axis is horizontal, y -axis is vertical.

structure to be topologically identical to that of the wolframite structure. Whereas in ZnWO_4 the Zn^{2+} ions are present in slightly axially compressed ZnO_6 octahedra, in CuWO_4 the Cu^{2+} ions are responsible for a significant Jahn-Teller distortion and impose a large axial elongation upon the CuO_6 octahedra. Despite the relatively undistorted form of the WO_6 octahedra, this Jahn-Teller effect is sufficient to cause a lowering of the monoclinic $P2_1/c$ symmetry to triclinic $P\bar{1}$ symmetry. It is interesting to note that Forsyth *et al.* (1991) have postulated a further reduction in symmetry of CuWO_4 to $P1$.

Experimental techniques

The samples, whose syntheses are described elsewhere (Schofield and Redfern, 1992), were thoroughly ground in an agate pestle and mortar and pressed into thin plastic sample holders using Sellotape windows to hold the samples in place. EXAFS spectra were recorded at the SERC Daresbury Synchrotron Radiation Source, operating in multibunch mode at an energy of 2 GeV, with an average current of 150 mA. Data were collected in transmission mode on station 7.1 using a double crystal Si(111) monochromator, detuned to give 50% rejection of the incident beam in order to reduce harmonic contamination. For data collected from samples containing lower proportions of the element measured, several scans (2–9) were collected and averaged to improve the signal-to-noise ratio. For experiments carried out at liquid nitrogen temperatures the samples were attached to aluminium holders, cooled in liquid nitrogen and placed in an evacuable cryostat

chamber. The temperature was maintained by conduction from a reservoir of liquid nitrogen.

The spectra were background subtracted and normalized by fitting polynomials to the pre-edge and the post-edge regions. The data were analysed in the program EXCURVE90 (Binsted *et al.*, 1990) utilizing single scattering curved wave theory (Lee and Pendry, 1975; Gurman *et al.*, 1984). Phase shifts were calculated in the program, using X-alpha potentials and the program default values for the muffin tin radii and ionicity. Theoretical spectra for end-member samples were generated by defining shells of backscatters using the known X-ray diffraction crystal structures (Filipenko *et al.*, 1968; Kihlberg and Gebert, 1970), and then iterating the distances, R , and the Debye-Waller factors, $2\sigma^2$, (where σ is the deviation of the interatomic distances between the absorber and the scatterer from its average value) to give the best agreement with the experimental spectra. The Joyner statistical test (Joyner *et al.*, 1987) was used on addition of each shell beyond the first, in order to check the significance of any improvement in the fit. Only shells with a statistical significance at the 1% level were included in the final fit.

Spectral analysis

The calculated phase shifts were checked against model compounds, in this case the end members CuWO_4 and ZnWO_4 . Bond lengths obtained from the EXAFS data and those determined from X-ray diffraction for CuWO_4 and ZnWO_4 are shown in Tables 1 and 2. By comparing Fig. 2 to the data in Tables 1 and 2 it can be seen that data can be fitted

TABLE 1. A comparison of the EXAFS model of ZnWO_4 with the X-ray diffraction data from Filipenko *et al.* (1968). CN is the coordination number, R (Å) is the distance from the central Zn atom to the shell, corrected for phase shifts in this table, and A (Å²) is the Debye-Waller factor.

Shell No.	ZnWO ₄ EXAFS Data				XRD Data	
	Atom	CN	R (Å)	A	R range	R_{av}
1	O	2	1.95	0.006	2.061	2.061
2	O	4	2.11	0.019	2.133–2.139	2.136
3	O	4	2.94	0.033	3.172	3.172
4	Zn	2	3.17	0.017	3.182–3.380	3.281
5	W	4	3.40	0.020	3.519–3.523	3.521
6	W	4	3.61	0.030	3.678–3.722	3.700
7	Zn	6	4.60	0.067	4.465–4.950	4.712
8	Zn	6	5.60	0.026	5.684–5.700	5.691
9	W	12	6.07	0.039	5.934–6.196	6.102
10	Zn	8	6.53	0.033	6.495–6.844	6.689
11	W	4	7.33	0.033	7.377–7.379	7.378
12	Zn	4	7.48	0.026	7.401	7.401

TABLE 2. A comparison of the EXAFS model of CuWO_4 with the X-ray diffraction data from Kihlborg and Gebert (1970). CN is the coordination number, R (\AA) is the distance from the central Cu atom to the shell, corrected for phase shifts in this table, and A (\AA^2) is the Debye-Waller factor.

Shell Nr.	CuWO ₄ EXAFS Data				XRD Data	
	Atom	CN	R (\AA)	A	R range	R_{av}
1	O	4	1.96	0.008	1.961–1.997	1.976
2	O	2	2.22	0.022	2.347–2.451	2.399
3	Cu	2	3.01	0.023	2.968–3.150	3.059
4	W	6	3.50	0.025	3.437–3.636	3.528
5	W	2	4.05	0.017	3.826–4.118	3.972
6	Cu	6	4.52	0.036	4.630–5.009	4.749
7	Cu	2	5.44	0.032	5.408–5.497	5.453
8	W	2	5.74	0.008	5.638–5.680	5.659
9	Cu	1	5.86	0.011	5.643	5.643

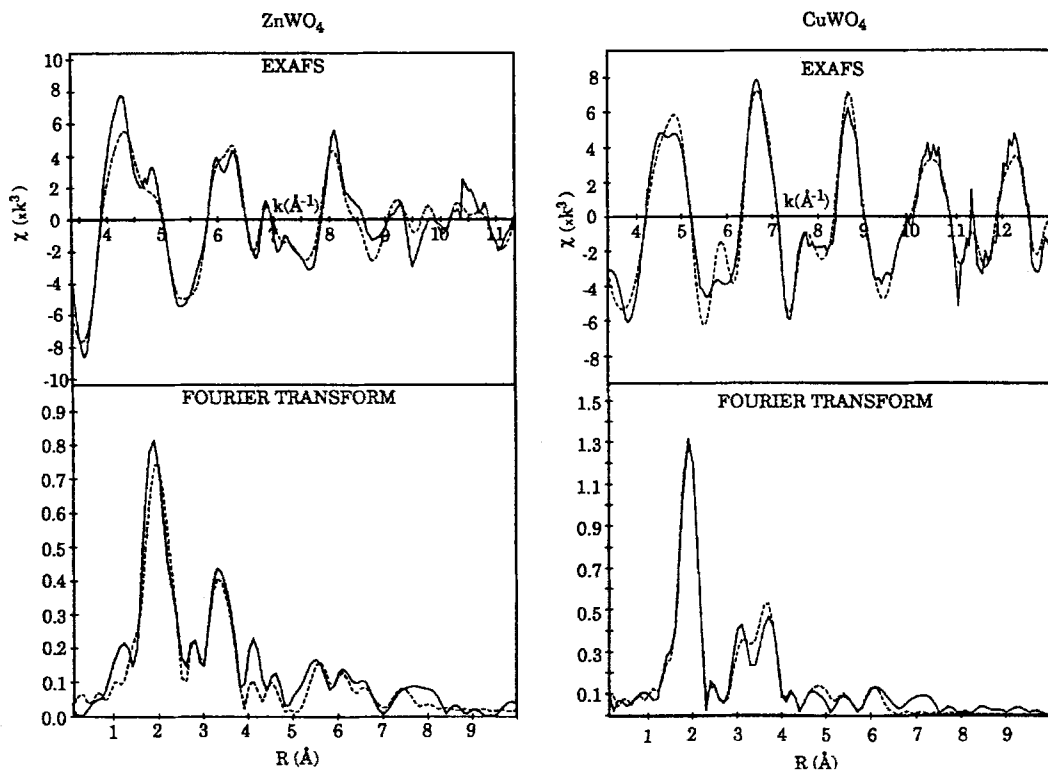


FIG. 2. The EXAFS (above) and Fourier transforms (below) of the end members ZnWO_4 (left) and CuWO_4 (right). The EXAFS have been multiplied by k^3 and the Fourier transforms have been corrected for phase shifts. The solid line represents the experimental EXAFS (or Fourier transform) and the dashed line represents the theoretical EXAFS (or Fourier transform).

out to about 7.5 Å in monoclinic ZnWO₄ but only to about 5.5 Å in triclinic CuWO₄. The broadened first peak in the Fourier transform for ZnWO₄ requires a split first shell of oxygens and the peak at about 3.1 Å is due to another oxygen shell; note that this last peak cannot be detected in CuWO₄ due to the lack of radial symmetry of the oxygen net about the Cu atoms in the triclinic CuWO₄ structure. The remaining peaks in both end members can be assigned to shells of metal backscatterers, Zn or Cu and W (Tables 1 and 2). Detailed analysis of the bond distances in these tables reveals significant differences between the EXAFS-derived value and the X-ray diffraction value for the first shell for ZnWO₄ and the second shell of CuWO₄ and it is felt that these discrepancies require further discussion.

Limitations of the EXAFS technique in the study of disordered systems have been discussed, for example, by Eisenberger and Brown (1979), Eisenberger and Lengeler (1980) and Brown *et al.* (1988). For systems in which static disorder is large, (≥ 0.1 Å) a reduction in the EXAFS amplitude and coordination numbers results, and an apparent contraction in the near-neighbour bond distances of up to 0.15 Å can be expected. The static disorder for the second shell of CuWO₄ can be seen to be large for the X-ray data in Table 2 and the addition of 0.15 Å to the second shell EXAFS bond distance brings the EXAFS derived value within the R range obtained from the X-ray diffraction study of Kihlberg and Gebert (1970). The static disorder in the first shell of ZnWO₄, however, is found to be zero from the X-ray diffraction study of Filipenko *et al.* (1968), Table 1, so the above arguments do not apply for ZnWO₄.

There are several plausible reasons for the apparent shortening of the EXAFS derived bond distance for the first oxygen shell in ZnWO₄. The first, and possibly the most important, is related to the reliability of the data from the X-ray diffraction data of Filipenko *et al.* (1968). Their brief communication gives no information about the purity of the starting compounds. However, the deep red colour of their ZnWO₄ single crystal possibly indicates the presence of impurities. Also their final R factor of 10% for the refinement is rather high, and they estimated the X-ray intensities visually. Finally, there is no mention of the thermal vibration assumptions made during the refinement; these may have a very significant effect. Indeed Abrahams (1967) has shown that for the refinement of α -ZnMoO₄, anisotropic thermal vibrations had to be assumed. Anisotropic thermal vibrations could also be responsible for an apparent reduction in the EXAFS bond distances

in the present study. Until a more detailed refinement of the ZnWO₄ structure is available, the quality of these bond distances cannot be rigorously checked. The Zn–O bond distances of approximately 1.95 Å are not unreasonable, especially where the coordination number is low. Abrahams (1967) has shown that in α -ZnMoO₄ the ZnO₅ polyhedra have Zn–O distances as small as 1.95 Å, and Simonov *et al.* (1977) found that the Zn–O distances within the ZnO₄ polyhedra in willemite, Zn₂SiO₄, are 1.96 Å.

Results

The experimental and calculated EXAFS and Fourier transforms for the end members ZnWO₄ and CuWO₄ are displayed in Fig. 2 and the radial shell information given in Tables 1 and 2. Best fits of the EXAFS for all intermediate compositions were obtained using the end-member models as starting points. For example, the room temperature Zn EXAFS for Zn_{0.9}Cu_{0.1}WO₄ was analysed by iterating the interatomic distances (denoted R values) and Debye-Waller factors (denoted A values) of the best fit model for the room temperature EXAFS of ZnWO₄. Once the R and A values had been obtained for the nearest neighbour oxygen shells which form the octahedral coordination environments, the R and A values for all the shells were iterated until a best fit for the whole model was obtained. The room temperature EXAFS of Zn_{0.8}Cu_{0.2}WO₄ was then analysed using the parameters from the best fit for Zn_{0.9}Cu_{0.1}WO₄ as a starting point. The parameters from the model for Zn_{0.8}Cu_{0.2}WO₄ were then used as a start for the analysis of the next sample in the solid solution series, and so on throughout the series.

Once the initial fitting of the EXAFS of the solid solution series was complete, the octahedral site geometry around the target atom was varied and the fitting process was repeated in order to assess the effects of different possible octahedral arrangements. The EXAFS analysis was constrained with three different near-neighbour oxygen arrangements, with coordination number ratios for the first two shells of 2:4, 4:2 and 6:0. The fit indices, R values and A values for the first two shells, which comprise the octahedral site around the target atom, are displayed in Tables 3–8. In several cases, where the target atom is present in very small concentrations, the data obtained are poor due to the small EXAFS signal, relatively low signal to noise ratio, and consequent problems in the background subtraction process. Despite many attempts at improving these experimental data, it has not been possible to extract any reliable data from the EXAFS of these samples.

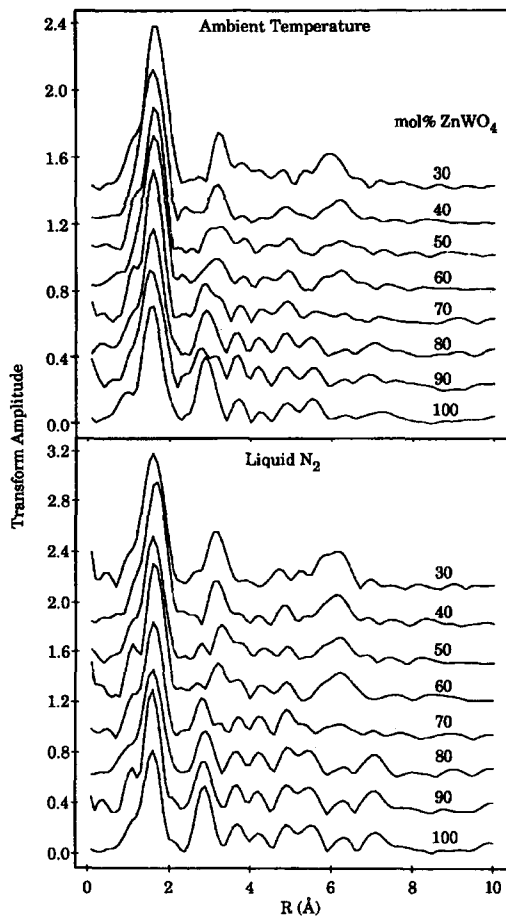


FIG. 3. Fourier transforms from Zn K-edge EXAFS of samples within the $(\text{Cu}_x\text{Zn}_{1-x})\text{WO}_4$ solid solution series collected at ambient (above) and liquid nitrogen (below) temperatures. Note that the trends described in the text are exemplified for both temperatures. Peak positions are not phase shift corrected.

The Debye-Waller factor is also a very useful parameter for comparing different models. In most cases this factor indicates the degree of disorder of a certain shell while the coordination number is a measure of the contribution made by that shell to the total EXAFS. However, where the coordination number is kept constant the magnitude of the Debye-Waller factor will also be a measure of the degree of contribution from a specific shell to the EXAFS. Essentially, the value of the Debye-Waller factor for a specific shell

varies inversely to the EXAFS contribution from that shell, and its value is dependent upon interatomic distance, coordination number and the degree of static and thermal disorder of the shell. As discussed in detail later, we have attempted to determine the geometry of distorted first oxygen shells about the target element by splitting the six nearest neighbour oxygens into two shells (i.e. 2:4, 4:2 and 6:0). In the EXAFS data refinement, the Debye-Waller factor and the coordination number are highly correlated. Thus we would expect that a shell with two oxygen atoms would have a proportionately lower Debye-Waller factor than a shell with four oxygen atoms. If this is not the case, the model might be suspect. In addition when a proposed two-shell model becomes unreasonable the computer iteration process tends to increase one Debye-Waller factor dramatically, while decreasing the other. Values for the Debye-Waller factors are clearly dependent upon the systems involved, however, the models for the two end members can be used to assess the reliability of values obtained for intermediate samples. Debye-Waller factors are generally quoted with a relative error of $\sim 20\%$.

Although bond distance information is a less sensitive indicator of the quality of a first shell oxygen model it is certainly not to be neglected. Brown *et al.* (1988) stated that, in general, this type of information has a reliable inter-shell resolution of 0.1 \AA , while Calas *et al.* (1990) stated that in favourable cases these distances can be obtained with an absolute accuracy of $\pm 0.02 \text{ \AA}$. The resolution of the EXAFS data is intrinsically dependent upon the k -range of the data collected and the nature of the problem under investigation. In particular the high k -values, being more sensitive to the shorter distance contributions. For example, where Fe^{3+} is present in a single FeO_6 octahedral site in both hematite and goethite, differences in the Fe-O interatomic distances of 0.17 \AA and 0.14 \AA , respectively, have been resolved confidently by Combes *et al.* (1986). The R values must be taken into account when comparing different models and will be described in more detail in the next section. In essence, however, it must be stated that, for this system, when the bond distances between two shells of the same atom type are within $\sim 0.1 \text{ \AA}$ it is unreasonable to maintain two independent shells.

Finally, in comparing information for the two end members, ZnWO_4 and CuWO_4 , structural information from X-ray diffraction studies has also been used as a criterion for assessing the different models. This information is presented in Tables 1 and 2.

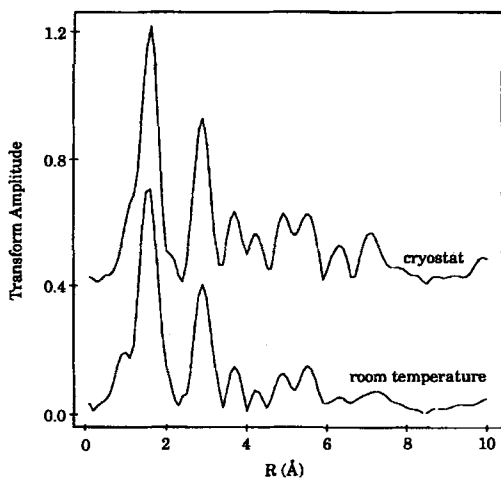


FIG. 4. A comparison of the Fourier transforms for ZnWO_4 at room and liquid nitrogen temperatures.

Discussion

In the following two sections the trends observed in the series of Fourier transforms for the Zn and Cu *K*-edge EXAFS will be discussed and correlated to systematic variations in the oxygen shells around the Zn and Cu target atoms. It is important to note that the Fourier transform series at both ambient and liquid nitrogen temperatures, displayed in Fig. 3 for Zn *K*-edge EXAFS and Fig. 5 for Cu *K*-edge EXAFS, have been used in a complementary fashion, in the observation, discussion and interpretation of the trends reported. Secondly, although the Fourier transforms of the ZnWO_4 and CuWO_4 end members shown in Fig. 2 have been corrected for phase shifts, the Fourier transforms in Figs. 3–6 are not phase shift corrected. An approximate correction can be applied by adding ~ 0.3 – 0.4 Å to the *R* values in these two Figures. The *R* values quoted in the following section are taken from Figs. 3 and 5 and, hence, are not phase shift corrected.

Zn K-Edge EXAFS

Several points of interest are revealed by the full series of Fourier transforms of the Zn *K*-edge EXAFS spectra (Fig. 3). As the Zn-content decreases, the amplitude of the first major peak of the Fourier transform increases. This peak corresponds to the first two oxygen shells forming the octahedron around the central Zn atom. Changes to the amplitude of this peak reflect

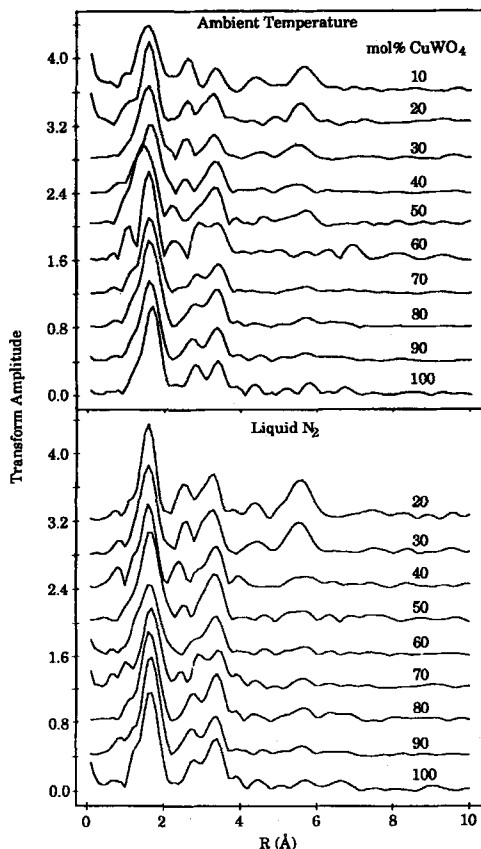


FIG. 5. Fourier transforms from Cu *K*-edge EXAFS of samples within the $(\text{Cu}_x\text{Zn}_{1-x})\text{WO}_4$ solid solution series collected at ambient (above) and liquid nitrogen (below) temperatures.

modification of the octahedral site geometry about the Zn atom and this relationship will be examined in more detail below.

By comparing the overall topologies of the Zn Fourier transforms for the solid-solution series (Fig. 3), a crucial point becomes clear. The Fourier transform of the ZnWO_4 end member EXAFS clearly represents the monoclinic arrangement of atom shells around the central Zn atom: note that peaks at 2.9 Å and 3.7 Å are diagnostic of this configuration. At the Cu-rich end of the series, the Zn Fourier transform for $\text{Zn}_{0.3}\text{Cu}_{0.7}\text{WO}_4$ can be considered as representative of the triclinic arrangement of atom shells about the central Zn atom: a peak at ~ 3.3 Å and troughs at 2.9 Å and 3.7 Å are diagnostic. With decreasing Zn content the peaks at 2.9 Å and 3.7 Å decrease in amplitude, while a peak with an intermediate *R*

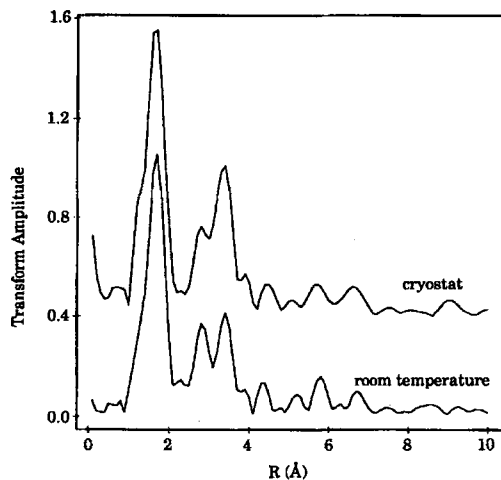


FIG. 6. A comparison of the Fourier transforms from Cu K-edge EXAFS of CuWO_4 at room and liquid nitrogen temperatures.

value (~ 3.3 Å) can be seen to increase in significance (in particular for samples $\text{Zn}_{0.6}\text{Cu}_{0.4}\text{WO}_4$ and $\text{Zn}_{0.7}\text{Cu}_{0.3}\text{WO}_4$). Based on the peak correlations given above, this implies two distorted Zn octahedral environments are present in the intermediate samples, one representing the 'microscopic'-monoclinic- and the other representing the 'microscopic'-triclinic-arrangement. The observed intensity trends for these three peaks in the Fourier transform series reflect that the ratio of monoclinic:triclinic-type sites decreases as the Zn-content decreases.

The three relevant peaks in the Fourier transform series can be assigned to specific metal shells with a reasonable degree of confidence and, in addition, changes in the Debye-Waller factors for these shells provide further useful information. Shell number 4 in Table 1 (Zn-Zn/Cu correlations) can be matched with the peak at ~ 2.9 Å (which becomes ~ 3.2 Å when corrected for phase shifts, as in Fig. 2 and Table 1) and assigned to the microscopically-monoclinic-type site. Its Debye-Waller factor increases from 0.017 to 0.034 as the Zn-content decreases pointing to a 'decreasing' contribution of this shell to the total EXAFS (see earlier section on assessment of different models). By contrast, the peak at ~ 3.3 Å (becoming ~ 3.5 Å when corrected for phase shifts), which is associated with the microscopically-triclinic-type site, can be assigned to shell numbers 5 and 6 in Table 1 (Zn-W correlations). Its Debye-Waller factor decreases from 0.030 to 0.010 with decreasing Zn pointing to an 'increasing' contribu-

tion of this shell to the total EXAFS. These trends in Debye-Waller factors are entirely consistent with the changing site proportions deduced above.

The peak at ~ 6 Å increases in amplitude as the Zn-content decreases and again this is reflected by the variation in the Debye-Waller factor of shell ten which decreases from 0.033 to 0.018. The peak at ~ 7.2 Å decreases as the Zn-content decreases to the point where it cannot be clearly distinguished from the background reflecting the reduction in the distance from which structural information is obtainable in the samples with the macroscopic radial shell distribution with overall triclinic symmetry.

If only the first coordination spheres forming the octahedral sites of the of the Zn atoms are considered, then the above interpretation (considering multiple shells) that two Zn sites are present can be assessed. Table 3 shows the fit indices for the whole of the EXAFS spectrum together with the bond distances (R) and the Debye-Waller factors (A) of the first two shells for different possible models across the solid solution. Throughout the series, octahedral site geometries with two short Zn-O bonds and four long Zn-O bonds (2:4) and also with four short Zn-O bonds and two long Zn-O bonds (4:2), both appear to be equally reasonable solutions but that for the model representing six equivalent Zn-O bonds (6:0) is less reasonable. Comparison with the X-ray diffraction data given in Table 1, however, shows that the 2:4 configuration is in fact likely to be the correct configuration for the single site present in ZnWO_4 . Using the criteria discussed in the previous section, in particular the relative values of Debye-Waller factors for the two oxygen shells, the arrangement 2:4 is, in fact, marginally better than the 4:2 arrangement for all the Zn-rich samples. In addition, the R_2 bond length for the 4:2 oxygen arrangement is unreasonably long for these Zn-rich samples (cf. XRD distances for the second shell in Table 1). Based on these same criteria in the Zn-poor samples, such as $\text{Zn}_{0.3}\text{Cu}_{0.7}\text{WO}_4$, the arrangement 4:2 appears more reasonable, a result which is consistent with the triclinic model for CuWO_4 , shown in Table 2.

As the Cu:Zn ratio approaches one, in the samples $\text{Zn}_x\text{Cu}_{1-x}\text{WO}_4$, where $x = 0.6, 0.5$ and 0.4 , the fit index (F.I.) value for the 6:0 model decreases significantly suggesting that an octahedral site geometry represented by six equal Zn-O bonds becomes as equally viable as the other two models. This can also be observed by the R values of the two shells in each of the 2:4 and 4:2 models becoming very similar. Although a single site with 6:0 geometry is a simple interpretation of the data,

the same result would be obtained if the two sites 2:4 and 4:2 were present in approximately equal proportions, due to the averaging nature of the EXAFS information.

The assessment of the variation in the degree of distortion of the ZnO_6 octahedra may be done in a simple manner by observing the variation in the difference between R_1 and R_2 ($\Delta = R_2 - R_1$). For the 2:4 arrangement, the dominant site in the Zn-rich samples, ΔR decreases continuously towards $\text{Zn}_{0.5}\text{Cu}_{0.5}\text{WO}_4$, where the two sites appear to be present in equal proportions, as would be expected due to the increase in proportion of the second site. Note that the decrease in ΔR is greatest between the samples $\text{Zn}_{0.8}\text{Cu}_{0.2}\text{WO}_4$ and $\text{Zn}_{0.75}\text{Cu}_{0.25}\text{WO}_4$. It is between these two samples that the phase transition occurs, destroying the long-range monoclinic symmetry, and so it could be expected that this transition would lead to a more dramatic change in the distortion of the ZnO_6 octahedra. In the region where the second site (with the 4:2 arrangement) is dominant, ΔR begins to increase again. This could reflect the increased proportion of this site as the macroscopic triclinicity of the sample increases dramatically (Schofield and Redfern, 1992).

Table 4 shows analogous data to that in Table 3 for experiments performed using a cryostat in which the sample is cooled to liquid nitrogen temperatures. Figure 4 shows a comparison of the Fourier transforms of the ZnWO_4 end member EXAFS from room temperature and liquid nitrogen temperature analysis. As can be seen in Fig. 4 all the major peaks in the Fourier transform for the cooled sample are significantly increased in amplitude. This change is reinforced by the fact that the Debye-Waller factors for all the shells, except the first two, show significant decreases for the cooled samples. This indicates that all these shells possess similar and significant thermal disorder effects which are reduced at low temperatures, revealing a more realistic view of the static disorder of the shells. The Debye-Waller factors of the first two shells, however, appear to indicate that a significant degree of static disorder is present at ambient and liquid nitrogen temperatures.

A comparison of the general topology and the trends seen in the series of Fourier transforms for the ambient and low temperature experiments in Fig. 3 reveals that the degree of static and thermal disorder is similar for all the samples in the solid solution.

From the data given in Table 3 a second possible interpretation, involving only a single octahedral ZnO_6 site might be considered plausible. In the ZnWO_4 end member and the

ZnWO_4 -rich samples, this site would possess the geometry described by the shell arrangement of 2:4. On addition of Cu, this octahedral site could distort until at a composition of approximately $\text{Zn}_{0.6}\text{Cu}_{0.4}\text{WO}_4$ the ZnO_6 octahedra might have become symmetrical, (6:0). Continued addition of Cu could cause these regular ZnO_6 octahedra to distort further into a 4:2 geometry, similar to that of the Jahn-Teller distorted CuO_6 site in CuWO_4 . However, this single-site structural explanation is not supported by the trends observed in the topologies of the Fourier transforms presented in Fig. 3. In sum, it appears that the progressive introduction of Cu into the ZnWO_4 structure creates an increasing proportion of a second Zn site in which the first two oxygen shells take on a geometry more comparable to the CuO_6 sites present in CuWO_4 . These new sites may well represent ZnO_6 octahedra in close vicinity to the strongly Jahn-Teller distorted CuO_6 sites. As the Cu-content increases, the proportion of the highly distorted site, with the arrangement 4:2, increases until the Zn:Cu ratio approaches unity. At this point the EXAFS analysis appears to indicate the existence of a symmetrical ZnO_6 site with six equal Zn-O bonds. However, this is interpreted to be a result of the average of the two Zn sites present in equal proportions. As the Cu-content continues to rise the 4:2 arrangement becomes dominant, indicating the preference of the structure to adopt a very distorted microscopically triclinic ZnO_6 site.

It is clear that the range of the solid solutions containing Zn-environments with two distinct local symmetries overlaps the monoclinic-triclinic phase transition detected at $\text{Zn}_{0.78}\text{Cu}_{0.22}\text{WO}_4$ using X-ray powder diffraction methods. This reflects the different length scales probed by the two techniques. It seems that monoclinic-to-triclinic site distortions occur initially on a local scale (denoted 'microscopic' in this paper) but that these distortions become ordered giving coherence on a long-range length scale, leading to the occurrence of the overall monoclinic-triclinic phase transition.

Cu K-edge EXAFS

Several trends also can be identified from the Fourier transforms of the Cu *K*-edge EXAFS in Fig. 5. Firstly, the intensity of the major peak in the Fourier transforms remains fairly constant as the Cu-content decreases to $\text{Zn}_{0.90}\text{Cu}_{0.10}\text{WO}_4$ where the intensity decreases dramatically. This peak is associated with the first two shells in the CuWO_4 model, Table 2. Together these shells represent the oxygen octahedron around the

central Cu atom. Thus it appears that no major change in the CuO_6 octahedra occurs until $\text{Zn}_{0.90}\text{Cu}_{0.10}\text{WO}_4$, a composition well into the region of stability of the macroscopic monoclinic symmetry. Indeed observation of the Fourier transform for the sample $\text{Zn}_{0.90}\text{Cu}_{0.10}\text{WO}_4$ shows it to be different in many respects from the Fourier transforms of the Cu-rich samples in this series. In Zn-dominated compositions this may reflect the complete compliance of CuO_6 octahedra with the geometrical characteristics of ZnO_6 octahedra as present in ZnWO_4 .

The second peak in the series of Fourier transforms, at ~ 2.8 Å, decreases in intensity and increases in R value with decreasing Cu-content to a point where it only shows as a shoulder on the third peak at $\text{Zn}_{0.70}\text{Cu}_{0.20}\text{WO}_4$. This decrease in intensity is accompanied by an increase in the Debye-Waller factor from 0.023 to 0.035. Comparison of the Tables 1 and 2 shows that the increase in the R value of this peak (with an X-ray diffraction derived value of 3.059 Å in CuWO_4) reflects the move toward monoclinicity of this shell where, in the ZnWO_4 end member, it has an X-ray diffraction-derived value of 3.28 Å. At the composition $\text{Zn}_{0.40}\text{Cu}_{0.60}\text{WO}_4$ a new peak appears at 2.6 Å and as the Cu-content decreases this peak increases in intensity becoming the second most intense peak in the Fourier transform of $\text{Zn}_{0.90}\text{Cu}_{0.10}\text{WO}_4$. This peak in the Fourier transform cannot be explained for the triclinic CuWO_4 model. However, the monoclinic ZnWO_4 model provides a good fit to this peak, and it can be attributed to the third shell of oxygen atoms which is essential in the model of ZnWO_4 (Table

1). This shell is not required in the model of the CuWO_4 EXAFS as the reduced symmetry of CuWO_4 increases the static disorder of the oxygen atoms, hindering any significant contribution from these oxygen atoms to the EXAFS. This shows that although the Jahn-Teller elongated CuO_6 octahedra appear to be very resistant to further distortion, the environments around these octahedra are not, and begin to approach the monoclinic shell arrangement well before the phase transition occurs at $\text{Zn}_{0.78}\text{Cu}_{0.22}\text{WO}_4$.

The intensity of the third peak, at ~ 3.4 Å, in the Fourier transforms remains fairly constant across the solid solution, however, as the Cu-content decreases this peak appears to broaden slightly up to a composition of $\text{Zn}_{0.80}\text{Cu}_{0.20}\text{WO}_4$ where two peaks maybe present. This feature may be correlated with Cu-W distances, represented by shells four and five in Table 2, which eventually re-order into shells five and six in the monoclinic model, Table 1.

The appearance of the two clear features at ~ 4.5 Å and ~ 5.6 Å in the Fourier transform for $\text{Zn}_{0.90}\text{Cu}_{0.10}\text{WO}_4$ reflect the change of the Cu environment to mimic that of the Zn environment in ZnWO_4 . They cannot be confidently assigned to specific shells in the ZnWO_4 model but might tentatively be correlated with shells seven, eight and nine in Table 1 based on their R values and low Debye-Waller factors in the fits obtained using the monoclinic model.

Tables 5 and 6 show the fit indices for the entire model and the interatomic distances (R) and Debye-Waller factors (A) for the first two shells for different CuO_6 site geometries. The parameters

TABLE 5. Room temperature Cu K -edge data using the triclinic model. 4:2 and 2:4 represent the coordination number ratios of the first and second shells respectively. F.I. is the fit index; R_1 and R_2 are the interatomic distances from the Cu target atom to the first and second shell respectively; A_1 and A_2 are the Debye-Waller factors for the first and second shell respectively.

	F.I.	4:2				2:4				
		R_1	A_1	R_2	A_2	R_1	A_1	R_2	A_2	
CuWO_4	1.69	1.96	0.008	2.22	0.022	1.71	1.96	0.001	2.03	0.064
$\text{Zn}_{0.1}\text{Cu}_{0.9}\text{WO}_4$	1.83	1.95	0.011	2.21	0.038	2.17	1.95	0.004	2.01	0.046
$\text{Zn}_{0.2}\text{Cu}_{0.8}\text{WO}_4$	1.61	1.96	0.009	2.20	0.038	2.16	1.95	0.002	2.01	0.056
$\text{Zn}_{0.3}\text{Cu}_{0.7}\text{WO}_4$	1.41	1.95	0.011	2.23	0.030	1.57	1.95	0.003	2.02	0.078
$\text{Zn}_{0.4}\text{Cu}_{0.6}\text{WO}_4$	6.35	1.95	0.008	2.17	0.010	6.37	1.94	0.002	2.08	0.032
$\text{Zn}_{0.5}\text{Cu}_{0.5}\text{WO}_4$	6.38	1.95	0.013	2.12	0.028	6.76	1.93	0.008	2.02	0.027
$\text{Zn}_{0.6}\text{Cu}_{0.4}\text{WO}_4$	2.10	1.98	0.011	2.24	0.020	2.50	1.97	0.004	2.07	0.059
$\text{Zn}_{0.7}\text{Cu}_{0.3}\text{WO}_4$	3.17	1.97	0.012	2.19	0.026	3.46	1.96	0.006	2.05	0.041
$\text{Zn}_{0.75}\text{Cu}_{0.25}\text{WO}_4$	3.09	1.98	0.012	2.21	0.022	3.50	1.96	0.006	2.08	0.041
$\text{Zn}_{0.8}\text{Cu}_{0.2}\text{WO}_4$	8.86	1.96	0.011	2.18	0.024	8.94	1.95	0.005	2.06	0.037
$\text{Zn}_{0.9}\text{Cu}_{0.1}\text{WO}_4$	6.24	1.97	0.015	2.16	0.042	4.92	1.96	0.011	2.03	0.037

TABLE 6. Room temperature Cu *K*-edge data using the monoclinic model. Other data as in Table 5.

	4:2					2:4				
	F.I.	R_1	A_1	R_2	A_2	F.I.	R_1	A_1	R_2	A_2
CuWO ₄	1.69	1.96	0.009	2.22	0.041	1.10	1.96	0.001	2.00	0.063
Zn _{0.1} Cu _{0.9} WO ₄	1.12	1.96	0.011	2.24	0.052					
Zn _{0.2} Cu _{0.8} WO ₄	0.72	1.96	0.009	2.23	0.055					
Zn _{0.3} Cu _{0.7} WO ₄	0.71	1.96	0.012	2.29	0.036	0.92	1.95	0.003	2.00	0.086
Zn _{0.4} Cu _{0.6} WO ₄	9.04	1.95	0.011	2.20	0.053	8.66	1.95	0.004	2.01	0.058
Zn _{0.5} Cu _{0.5} WO ₄	6.77	1.95	0.013	2.11	0.031	7.19	1.93	0.008	2.02	0.031
Zn _{0.6} Cu _{0.4} WO ₄	1.72	1.98	0.011	2.25	0.030	1.55	1.98	0.004	2.03	0.071
Zn _{0.7} Cu _{0.3} WO ₄	1.28	1.97	0.012	2.22	0.032	1.71	1.96	0.005	2.05	0.055
Zn _{0.75} Cu _{0.25} WO ₄	2.00	1.97	0.011	2.20	0.021	2.20	1.96	0.007	2.07	0.047
Zn _{0.8} Cu _{0.2} WO ₄	5.53	1.96	0.010	2.18	0.024	4.85	1.96	0.005	2.04	0.040
Zn _{0.9} Cu _{0.1} WO ₄	4.99	1.98	0.016	2.15	0.087	5.29	1.97	0.011	2.01	0.042

shown result from the best fits of the room temperature Cu *K*-edge EXAFS using the CuWO₄ (triclinic) and the ZnWO₄ (monoclinic) end member models. Using the criteria discussed earlier, Table 5 shows that in all samples displaying macroscopically triclinic symmetry, a Jahn-Teller distorted oxygen arrangement of 4:2 is the most suitable despite the large rearrangement of the surrounding shells. By comparison, fit indices obtained using the triclinic models are inferior for the macroscopically monoclinic samples (i.e. Zn_{0.80}Cu_{0.20}WO₄ and Zn_{0.90}Cu_{0.10}WO₄).

Table 6 reveals similar data to those in Table 5, except that the twelve shell monoclinic model has been used instead of the nine shell triclinic model. In the majority of cases the fit indices are substantially improved upon those in Table 5, however, assessment of the Debye-Waller factors for most of these fits reveals unreliable results. The second shell of the 4:2 model only has a coordination number of two, hence, values between 0.04–0.05 are unrealistic. For the 2:4 model, on the other hand, the Debye-Waller factors for the first shell have been iterated to a very small value, whereas the corresponding value for shell two is unrealistically large for a shell containing four atoms at an *R* value of <2 Å. Nevertheless it can be seen that, particularly for the Cu-poor samples, the 4:2 model is superior to the 2:4 model. Due to the lower symmetry of the CuWO₄ structure, the radial information beyond ~5.9 Å becomes very difficult to model. Many shells would contain single atoms or several atoms covering a large *R* range, resulting in multiple overlapping shells. These problems combined with the relatively small amount of information revealed by the Fourier transforms above ~5.9 Å mean that the monoclinic model possesses a

larger number of shells than the triclinic model and hence the fit indices will inevitably be lower for the monoclinic model.

The fits for the 4:2 geometry employing the monoclinic model near to the phase transition, for example Zn_{*x*}Cu_{1-*x*}WO₄ where *x* = 0.6–0.75, do become acceptable and represent the appearance of certain monoclinic features in the local environment beyond the CuO₆ octahedra. Across the majority of the Fourier transform series the amplitudes of the first peak are relatively constant, however, between the samples Zn_{0.80}Cu_{0.20}WO₄ and Zn_{0.90}Cu_{0.10}WO₄ a sudden decrease in this amplitude can be observed. It has already been demonstrated that the first peak in the Fourier transform is related to the first two shells in the EXAFS model. These shells represent the oxygen octahedra around the Cu target atom, hence, this intensity change might tentatively be associated with a change in the Cu site symmetry from the Jahn-Teller tetragonally elongated 4:2 form to the 2:4 form more typical of the ZnO₆ octahedra in ZnWO₄. Again this conclusion may tentatively be derived from the data in Table 6 for the samples Zn_{0.80}Cu_{0.20}WO₄ and Zn_{0.90}Cu_{0.10}WO₄.

Comparison of the room temperature and the liquid nitrogen temperature data for pure CuWO₄ (Fig. 6) reveals a significant increase in the amplitude of the third major peak of the Fourier transforms. This peak is attributed to Cu–W interactions (shells four and five) and the increase in amplitude of this peak on cooling correlates with a decrease in the Debye-Waller factor for shell four from 0.025 to 0.018. This amplitude variation may represent a large thermal disorder contribution from the W shell relative to the other shells. A comparison of the Fourier transforms of the solid solution series at ambient and liquid

TABLE 7. Low-temperature Cu *K*-edge data using the triclinic model. Other data as in Table 5.

	4:2					2:4				
	F.I.	R_1	A_1	R_2	A_2	F.I.	R_1	A_1	R_2	A_2
CuWO ₄	3.45	1.96	0.008	2.26	0.038	4.20	1.95	0.001	1.98	0.049
Zn _{0.1} Cu _{0.9} WO ₄	3.43	1.96	0.007	2.28	0.030	3.68	1.96	0.000	1.99	0.072
Zn _{0.2} Cu _{0.8} WO ₄	3.03	1.95	0.008	2.23	0.029	3.67	1.95	0.001	2.03	0.065
Zn _{0.3} Cu _{0.7} WO ₄	8.04	1.97	0.008	2.26	0.010	9.48	1.97	0.001	2.05	0.076
Zn _{0.4} Cu _{0.6} WO ₄	2.33	1.97	0.012	2.27	0.026	2.72	1.96	0.005	2.02	0.059
Zn _{0.5} Cu _{0.5} WO ₄	4.77	1.97	0.008	2.24	0.022	5.57	1.96	0.002	2.02	0.054
Zn _{0.6} Cu _{0.4} WO ₄	5.81	1.96	0.008	2.18	0.013	4.95	1.94	0.000	2.09	0.035
Zn _{0.65} Cu _{0.35} WO ₄	6.85	1.98	0.016	2.24	0.032	7.38	1.96	0.010	2.05	0.048
Zn _{0.7} Cu _{0.3} WO ₄	8.81	1.95	0.009	2.17	0.026	8.76	1.95	0.003	2.04	0.039
Zn _{0.75} Cu _{0.25} WO ₄	7.82	1.96	0.009	2.18	0.022	8.14	1.96	0.003	2.04	0.037
Zn _{0.8} Cu _{0.2} WO ₄	13.37	1.96	0.006	2.17	0.006	13.20	1.95	0.000	2.10	0.025

nitrogen temperatures shows that the same trends are present in both series of experiments but the amplitude of the third peak is enhanced throughout the low temperature series, Fig. 5. Tables 7 and 8 also provide a similar interpretation to that of the room-temperature data of Tables 5 and 6.

In contrast to the Zn EXAFS results, the Cu EXAFS data show no obvious signs of the presence of two sites. However, Schofield *et al.* (1993) have recently used Cu *2p* absorption spectroscopy to show the presence of two distinct Cu electronic environments in this solid solution series. It seems that, with respect to these tungstates, the latter technique is the more sensitive probe, able to detect the subtle differences in Cu sites.

Conclusions

Interpretation of the Zn *K*-edge EXAFS has shown that the substitution of Cu into the ZnWO₄ structure generates a second octahedral Zn site. While the ZnO₆ octahedra in ZnWO₄ are axially compressed, intermediate samples in the solid-solution series possess a second ZnO₆ site that is axially elongate; and the relative proportions of the two sites varies progressively with composition. The relative geometries of these sites are schematically displayed in Fig. 7.

In contrast, Cu *K*-edge EXAFS show no clear evidence for two sites, rather the CuO₆ octahedra appear to maintain their axially elongate Jahn-Teller distorted geometry throughout the majority of the series. However, it is possible that the most Cu-deficient samples have a CuO₆ octahedral

TABLE 8. Low-temperature Cu *K*-edge data using the monoclinic model. Other data as in Table 5.

	4:2					2:4				
	F.I.	R_1	A_1	R_2	A_2	F.I.	R_1	A_1	R_2	A_2
CuWO ₄	1.89	1.95	0.008	2.35	0.056	3.44	1.95	0.000	2.66	0.058
Zn _{0.1} Cu _{0.9} WO ₄	1.93	1.96	0.007	2.30	0.039					
Zn _{0.2} Cu _{0.8} WO ₄	1.67	1.95	0.009	2.24	0.042					
Zn _{0.3} Cu _{0.7} WO ₄	4.34	1.96	0.009	2.29	0.028					
Zn _{0.4} Cu _{0.6} WO ₄	1.24	1.97	0.013	2.29	0.043					
Zn _{0.5} Cu _{0.5} WO ₄	2.81	1.97	0.008	2.25	0.042					
Zn _{0.6} Cu _{0.4} WO ₄	4.69	1.96	0.009	2.18	0.016	3.94	1.95	0.002	2.09	0.053
Zn _{0.65} Cu _{0.35} WO ₄	3.21	1.98	0.015	2.26	0.034	3.67	1.97	0.009	2.03	0.067
Zn _{0.7} Cu _{0.3} WO ₄	3.54	1.96	0.009	2.15	0.028	3.78	1.95	0.003	2.02	0.042
Zn _{0.75} Cu _{0.25} WO ₄	2.19	1.96	0.010	2.15	0.029	2.43	1.96	0.004	2.02	0.042
Zn _{0.8} Cu _{0.2} WO ₄	6.86	1.97	0.005	2.18	0.005	6.06	1.94	0.000	2.08	0.029

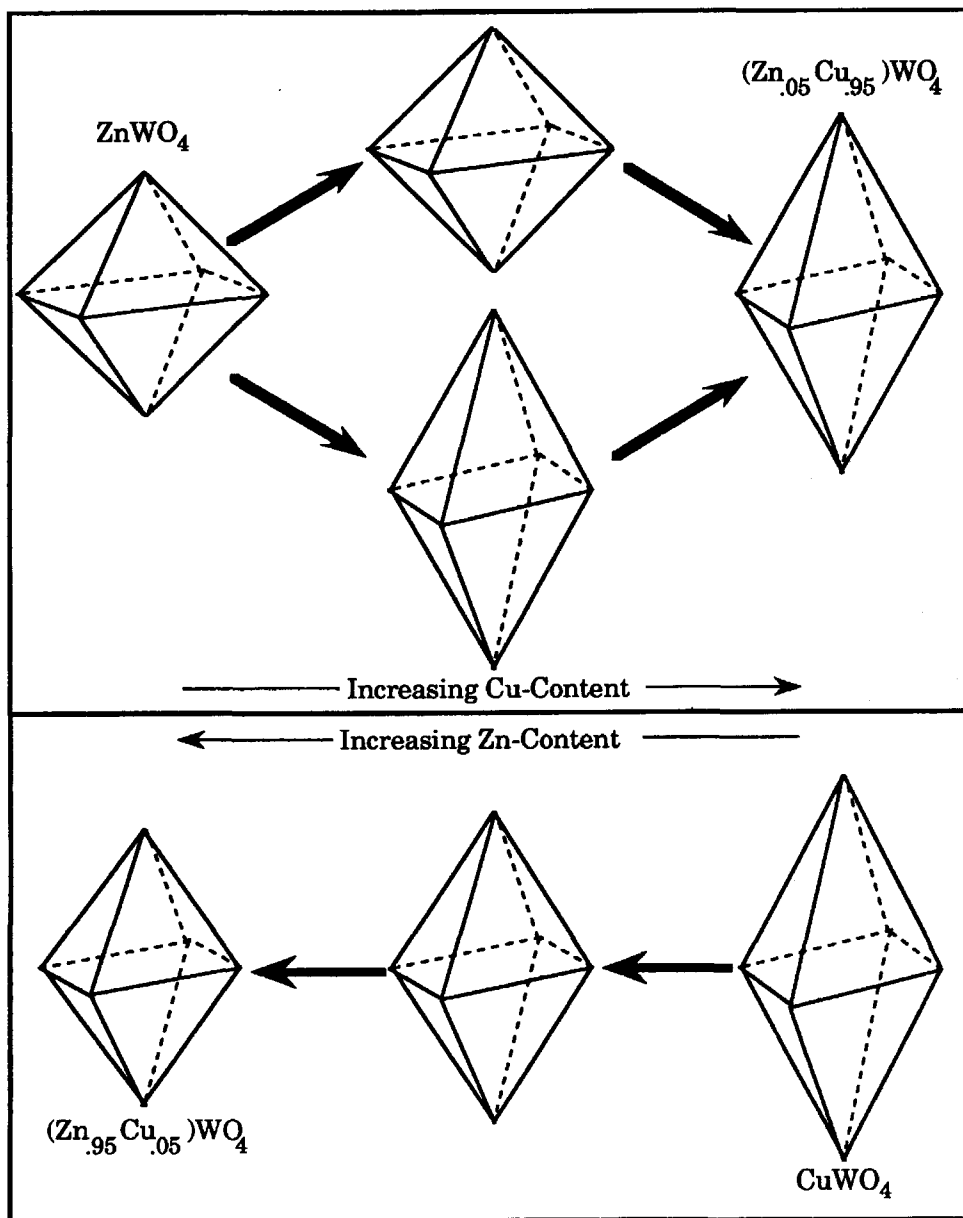


FIG. 7. Schematic representation of Zn environments (above) and Cu environments (below) in the $(\text{Cu}_x\text{Zn}_{1-x})\text{WO}_4$ solid solution series.

geometry more similar to that of the ZnO_6 in pure ZnWO_4 (Fig. 7). Recent Cu $2p$ absorption spectroscopy has provided unequivocal evidence for the presence of two subtly different Cu electronic environments in these samples (Schofield *et al.*, 1993).

Comparison of room and liquid nitrogen temperature K -edge EXAFS spectra shows that Zn sites are surrounded by shells of atoms which have similar relative thermal-to-static disorder contributions. In contrast, W shells surrounding Cu at ~ 3.50 – 4.05 Å have a large thermal disorder contribution.

A combination of XAS and XRD studies of the same samples has provided information about the short-range and the long-range structures, respectively. The interesting conclusion is that substitution of Cu for Zn (or vice-versa) involves local site modifications such that microscopically triclinic (or microscopically monoclinic) sites are introduced in advance of the displacive monoclinic-triclinic (or vice-versa) structural phase transition. Such an interpretation is only possible due to the utilisation of the complementary X-ray spectroscopic and diffraction techniques in this work.

Acknowledgements

P.F.S. is grateful to the NERC for the funding of a studentship. All the authors are grateful to the SERC for synchrotron beamtime allocations (BAP 19/34 and 20/109).

References

- Abrahams, S. C. (1967) Crystal structure of the transition-metal molybdates and tungstates. III Diamagnetic αZnMoO_4 . *J. Chem. Phys.*, **46**, 2052–63.
- Brown, G. E. Jr., Calas G., Waychunas G. A. and Petiau, J. (1988) X-ray absorption spectroscopy: Applications in mineralogy and geochemistry. In *Spectroscopic Methods in Mineralogy and Geology*. Mineralogical Society of America, *Reviews in Mineralogy*, **18**, (Hawthorne, F. C., ed.), 431–512.
- Binsted, N., Campbell, J. W., Gurman, S. J. and Stephenson, P. C. (1990) *SERC Daresbury Laboratory EXCURVE90 program*.
- Calas, G., Manceau, A., Combes, J.-M. and Farge, F. (1990) Application of EXAFS in mineralogy. In *Absorption Spectroscopy in Mineralogy*. (Mottana, A. and Burragato, F., eds.), 172–5.
- Combes, J. M., Manceau, G. and Calas G. (1986) Study of the structure in poorly-ordered precursors of iron oxi-hydroxides. *J. Physique*, **47**, 697–701
- Eisenberger, P. and Brown, G. S. (1979) The study of disordered systems by EXAFS: Limitations. *Sol. Stat. Commun.*, **29**, 481–4.
- Eisenberger, P. and Lengeler, B. (1980) Extended X-ray absorption fine structure determinations of coordination numbers: Limitations. *Phys. Rev.*, **B22**, 3551–62.
- Filipenko, O. S., Pobedimskay, E. A. and Belov, N. V. (1968) The crystal structure of ZnWO_4 . *Sov. Phys. Crystallogr.*, **13**, 127–9.
- Forsyth, J. B., Wilkinson, C. and Zvyagin, A. I. (1991) The antiferromagnetic structure of copper tungstate, CuWO_4 . *J. Phys.: Condens. Matter*, **3**, 8433–40.
- Gurman, S. J., Binsted, N. and Ross, I. (1984) A rapid, exact, curved wave theory for EXAFS calculations. *J. Phys. C: Solid State Phys.*, **17**, 143–51.
- Joyner R. W., Martin, K. J. and Meehan, P. (1987) Some applications of statistical tests in analysis of EXAFS and SEXAFS data. *J. Phys. C: Solid State Phys.*, **20**, 4005–12.
- Kihlborg, L. and Gebert, E. (1970) CuWO_4 a distorted wolframite-type structure. *Acta Crystallogr.*, **B26**, 1020–5.
- Klein, S. and Weitzel, H. (1975) PERNOD — ein Programm zur von Kristallstrukturparametern aus Neutronenbeugungspulverdiagrammen. *J. Appl. Crystallogr.*, **8**, 54–9.
- Lee, P. A. and Pendry, J. B. (1975) Theory of the extended X-ray absorption fine structure. *Phys. Rev.*, **B11**, 2795–811.
- Schofield, P. F. and Redfern, S. A. T. (1992) Ferroelastic phase transition in the sanmartinite (ZnWO_4)–cuproscheelite (CuWO_4) solid solution. *J. Phys.: Condens. Matter*, **4**, 375–88.
- Schofield, P. F. and Redfern, S. A. T. (1993) Temperature and composition-dependence of the ferroelastic phase transition in $(\text{Cu}_x\text{Zn}_{1-x})\text{WO}_4$. *J. Phys. Chem. Solids*, **54**, 161–70.
- Schofield, P. F., Henderson, C. M. B., Redlern, S. A. T. and van der Laan, G. (1993) Cu 2p absorption spectroscopy as a probe for the site occupancies of $(\text{Zn}_x\text{Cu}_{1-x})\text{WO}_4$ solid solution. *Phys. Chem. Minerals*, **20**, 375–81.
- Simonov, M. A., Sandomerskii, P. A., Egorov-Tismenko, Yu. K. and Belov, N. V. (1977) Crystal structure of willemite, Zn_2SiO_4 . *Sov. Phys. Dokl.*, **22**, 622–3.

[Manuscript received 11 May 1993;
revised 21 July 1993]